Optical properties of hexagonally arranged triangular arrays of Au-Ag nanoparticles

JIACHUN ZHENG[a], JING LIU[a,b,c,*], XIAOYI CHEN[d], HAOYUAN CAI[a], LINGQI KONG[b,c]
[a]*School of Information Engineering, Jimei University, Xiamen, Fujian 361021, PR China*
[b]*Department of Physics, Xiamen University, Xiamen, Fujian 361005, PR China*
[c]*China–Australia Joint Laboratory for Functional Nanomaterials, Xiamen University, Xiamen, Fujian 361005, PR China*
[d]*Department of Physics, National University of Singapore, Singapore 117551, Singapore*

Optical properties of hexagonally arranged triangular arrays of Au-Ag nanoparticles are systematically investigated. A gold thin film is deposited on top of the silver nanoparticles supported with substrate. The hybrid nanoparticles can prevent pure silver nanoparticles from oxidation and the stability of the hybrid Au-Ag nanoparticles compared with pure silver nanoparticles has been verified. Influence of the particle thickness on the extinction spectrum is studied and optimized through discrete dipole approximation (DDA) method and nanosphere lithography (NSL). Considering the nano-fabrication condition, 40 nm thickness is selected and the array is fabricated. The experimental results demonstrate that the measured spectrums are basically in agreement with the theoretical spectrums derived by the DDA calculation.

1. Introduction

Noble metal nanoparticles are well known for their ability to exhibit localized surface plasmon resonance (LSPR) which can be applied in surface-enhanced spectroscopy, [1] optical filters, [2] and plasmonic devices [3] etc. The LSPR refers to the excitation of surface plasmons by light from nanometer-sized metallic particles. The position and intensity of LSPR spectrum peaks are sensitively dependent on composition, size, shape, and inter-particle spacing of the nanoparticles as well as the dielectric properties of their local environments. [4-9] The discrete dipole approximation (DDA) is one of the most efficient computational numerical algorithms to simulate LSPR for the nanostructures with arbitrary shapes and dimensions. This method has significant advantages of occupying less computation resource, calculating the mutual action between the light and the metal nanostructures. [10-12] On the other hand, the nanosphere lithography (NSL) is the most low-cost, high-throughput method for producing periodic, geometrically tunable nanostructure arrays. [13-15] The NSL makes use of a template formed by the self-assembly of monodisperse nanospheres on flat surface acting as a deposition/etching mask.

However, most of metallic nanoparticles are designed on the basis of pure silver thin film metallic nanostructures. Corrosion-induced electrochemical damage on surface of the silver film exists at ambient atmosphere, especially in the period of time after micro/nanofabrication. The corrosion originates from oxidation which is well known for bulk silver. But for the silver thin film, dielectric constant of the silver thin film will be definitely changed due to the oxidation. Optical performance of the nanophotonic devices varies accordingly. To overcome this problem, we concentrate on the hybrid Au-Ag nanoparticle arrays in this paper. Moreover, metallic nanoparticle arrays with different thicknesses are of particular importance for surface Plasmon resonances and couplings, hence affecting photon flow accordingly.

In this paper, a new hexagonally arranged triangular Au-Ag nanoparticle arrays is put forth for preventing pure silver nanoparticles from oxidation. Using DDA algorithm to aid design parameters of the nanoparticle arrays is adopted for the model design. We develop an extended NSL method to fabricate the hybrid nanoparticle arrays with different thicknesses.

2. Model design

Using the DDA algorithm, we model the hexagonally arranged triangular hybrid Au-Ag nanoparticle arrays. Figs. 1 is schematic illustration of the hybrid Au-Ag triangular nanoparticle arrays in the DDA simulation. The hybrid Au-Ag nanostructures have an in-plane width of 130 nm and an out-of-plane height of 40 nm. The angle of the arris underside is $\alpha=60^{\circ}$. The gold film thickness are fixed on 5 nm and the thicknesses of triangular structure are changed from 25 nm to 60 nm. The use of periodic boundary

condition can reduce a higher computational cost and a bigger numerical model. The periodic boundary condition is contained in DDSCAT.7.3.0 reported by Draine and Flatau. [16] We model the experimental system by DDSCAT.7.3.0. The dielectric constants for gold and silver are cited from ref. 17. The size of the dipole is 2 nm which can promise the perfect convergence of the calculated results [17] and the higher calculated efficiency.

Extinction is a term used in physics to describe the absorption and scattering of electromagnetic radiation. Any changes in the parameters of metal nanoparticles could lead to the optical drift in extinction spectrum and thus influence the optical applications in practice [18-21]. Therefore, it is important to analyze the influence of the varied thickness on extinction. The calculated extinction spectra of different thicknesses is presented in Fig. 2. In these calculations, the gold film thickness are fixed on 5 nm and the thicknesses of triangular structure are 25, 30, 35, 40, 45, 50, 55 and 60 nm, respectively. Considering a reasonable number for the computation power and better result, in DDA calculation, the 2nm size of the dipole is used among the thicknesses of 25, 30, 35, 40 and 45 nm. The 3nm size of the dipole is used among the thicknesses of 50, 55 and 60 nm. When the thicknesses are changed to be 25, 30, 35, 40, 45, 50, 55 and 60 nm, respectively. The numbers of dipoles are 21984, 27480, 31144, 36640, 40304, 13838, 14652 and 16280, respectively. Fig. 2(a) shows the extinction spectra of hexagonally arranged triangular hybrid Au-Ag nanoparticle arrays with thicknesses changed to be 25, 30, 35, 40, 45, 50, 55 and 60 nm. When the thicknesses are change to be 25 nm, 30 nm and 50 nm, respectively. The corresponding positions of the peak wavelengths are located in 727 nm, 707 nm and 675 nm, respectively. When the thicknesses are 35 nm, 40 nm and 45 nm, the positions of the peak wavelengths are located in 687 nm. The peak wavelengths of 55 nm and 60 nm thicknesses are located in 649 nm. The relationship between the peak wavelengths and the thicknesses of the triangular hybrid Au-Ag particles is shown in Fig. 2(b), in which the influence of thicknesses on the positions of the peaks is shown. The relationship between the extinction efficiency and thickness of the triangular hybrid Au-Ag particles is shown in Fig. 2(c). As can be seen from Figs. 2(a)-2(c), when the thicknesses are 35 nm, 40 nm and 45 nm, the peak wavelengths are located in 687 nm. The extinction efficiency keeps relatively high value (the value less descended) and the corresponding full width at half maximum (FWHM) of the spectrum is narrower than other thicknesses. The thickness of 35-45 nm can be used as the structure parameter for our calculation.
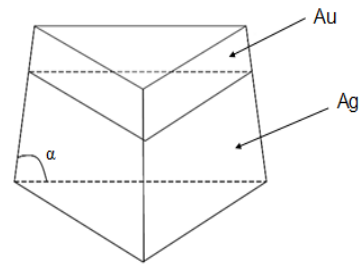
Fig. 1. Schematic illustration of the hybrid Au-Ag triangular nanoparticle arrays in the DDA simulation.
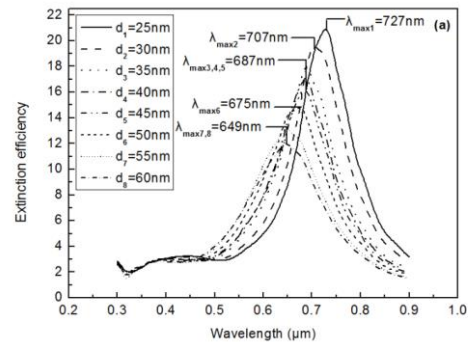
(a)
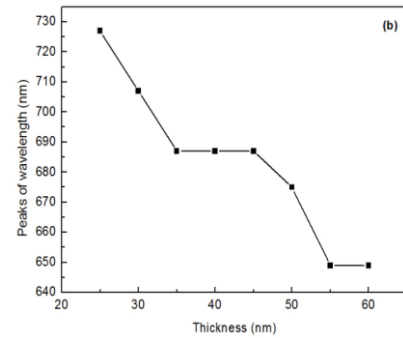
(b)
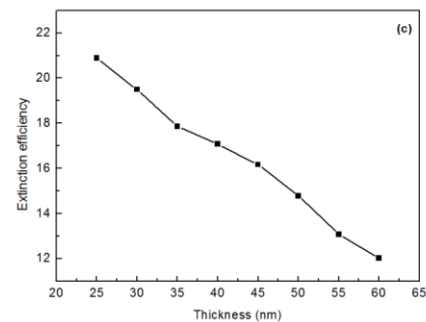
(c)

Fig. 2(a). Extinction spectra of hexagonally arranged triangular hybrid Au-Ag nanoparticle arrays for different thicknesses. (b) Relationship between the peaks of wavelength and the thicknesses of triangular hybrid Au-Ag particles. (c) Relationship between the extinction efficiency of wavelength and the thicknesses of triangular hybrid Au-Ag particles.

3. Fabrication of nanostructures

In our experiments, the triangular metal nanostructures with different thicknesses are fabricated by means of a NSL technique. The PS with a mean diameter of 260 nm [22] and a concentration of 10 wt% in solution are purchased from Suzhou Nano–Micro Bio-Tech Co. Ltd. First of all, close-packed nanosphere is a prerequisite. The regular monolayer as a deposition mask is principal to achieve large-area hexagonal structure. To begin with, the PS solution is diluted to be 3 wt% with deionized water. The glass substrates are thoroughly cleaned, in toluene, acetone, ethanol for 10 min respectively, then in piranha solution (H_2SO_4 : H_2O_2 = 3:1) for 2 hours to remove organic residues. To achieve a hydrophilic surface, the glass substrates are ultrasonically bathed in NH_4OH, H_2O_2, and H_2O solution with the ratio of 1:1:5 for 2 hours. Every sonication followed rinsing with large amount of deionized water. The cleaned surstrates are stored in deionized water until used.

Following drop-coating of the PS nanospheres on the substrate, chromium, silver and gold layers, are deposited on the PS mask sequentially, as shown in Fig. 3.

The deposition of gold (99.9%), silver (99.9%) and chromium (99.9%) is performed in a home-built thermal evaporator at a pressure of 5.0×10^{-4} Pa. The substrates are rotated at a speeds of 16.5 rpm all through the deposition. To achieve homogeneous deposition, the power for heating up of the source materials is carefully increased. The deposition rate is ~ 2.5 nm/s for gold and silver layers. and ~ 4.0 nm/s for chromium film.

The thickness has been monitored using a Dektak 3 Series surface profiler to achieve an identical depth for a low reflectance. It is controlled to be 5 nm for gold, and 25, 30, 35, 40 nm for silver films, respectively. After the deposition of gold film, the PS spheres are lifted off by immersing in absolute ethanol for about 5s. The PS are removed by sonication (B3500S-MT, Branson, 140W, 42 khz) in absolute ethanol. Nanostructures of the achieved PS mask and the hybrid Au-Ag nanoparticle arrays are characterized by LEO-1530 SEM and SPI-400 AFM. Ultravioletvisible (UV-vis) mirror reflection spectra are obtained on a Varian Cary 5000 UV-Vis-NIR spectrophotometer.
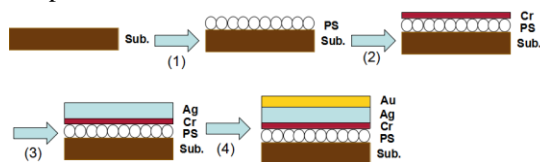
Fig. 3. Schematic illustration of hybrid Au-Ag nanoparticle array fabrication with the following four steps: (1) drop-coating of monolayered PS nanospheres on substrate; (2) deposition of a thin buffer layer of Cr film over the as-coated monolayered PS nanospheres; (3) a further deposition of a layer of Ag film following the Cr deposition; (4) final deposition of a caped layer of Au thin film on top of the Ag film.
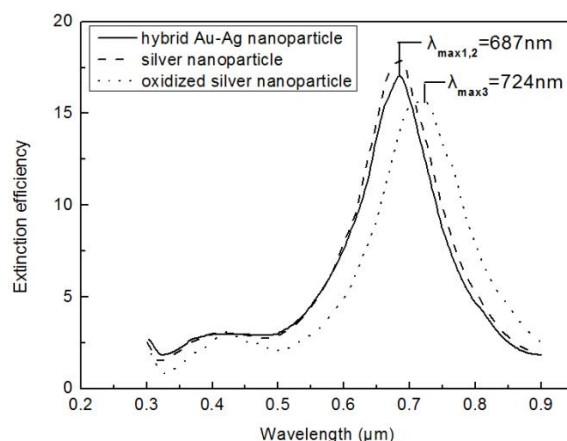
Fig. 4. Calculated spectra of arrays of (Dash) pure silver nanoparticle and (Solid) hybrid Au-Ag nanoparticle and (Dot) silver nanoparticle coated by silver oxide layer.

4. Result and discussion

We use DDA and NSL method to investigate the stability of the Au-Ag nanoparticles compared with pure silver nanoparticles.

NSL method are used to fabricate pure silver nanoparticle arrays (A array) and hybrid Au-Ag nanoparticle arrays (B array). The silver layer thickness of A array is 40 nm and B array has a thickness of silver 35 nm and gold 5 nm. Spectroscopic Ellipsometer (SpecEl-2000-VIS, measuring film thickness between 0.1 nm to 8 μm, the precision of 1 nm) is used to measure the thickness of two arrays exposed to air. The measured results show the thickness of oxidized silver layer in A array is about 5 nm and silver layer is about 38 nm. The total thickness of B array is not changed. The main component of the oxidized silver layer is Ag_2O and there may also be a small amout of other compounds.

In DDA calculation, we use the corresponding size of two arrays in experiments to calculate extinction spectras. The array has a thickness of Ag_2O 5 nm and silver 38 nm. Fig. 4 shows calculated spectra of arrays of (a) pure silver nanoparticle and (b) hybrid Au-Ag nanoparticle and (c) silver nanoparticle coated by silver oxide layer. As shown in Fig. 4, the positions of peak wavelengths of pure silver and hybrid Au-Ag nanoparticle are located in 687 nm and the intensity of the extinction of pure silver nanoparticle slightly appears increase. Because of the oxidation of silver nanoparticle, the intensity of the extinction obviously decreases and the peak position appears 37 nm redshift. The result show the existence of oxidized silver nanoparticle changes the optical properties.

Fig. 5 shows the SEM images of the pure silver and hybrid Au-Ag nanoparticle arrays. Two nanoparticle arrays both form a large-scale monolayer array with the hexagonally close-packed structure and have similar

nanoparticles morphology, as shown in Fig. 5. We have detected the UV–vis spectra of pure silver and hybrid Au-Ag nanoparticle arrays and the measured results are shown in Fig. 6. From Fig. 6, after arrays are coated with gold film, we compared the hybrid arrays with pure silver nanoparticle array, and finded that the positions of peak wavelengths of the hybrid Au-Ag nanoparticle array is not shifted, and the waveforms of two spectras are similar. The main reason is that the gold thickness is relatively thin compared to the silver thickness. After the samples of pure silver and hybrid Au-Ag nanoparticle arrays are exposed to air, we detect the UV–vis spectra of the samples and the measure results are shown in Fig. 7. The intensity of the extinction of oxidized silver nanoparticle arrays obviously decreases and the peak position appears 29 nm redshift compared to the hybrid Au-Ag nanoparticle arrays, as shown in Fig. 7. We can conclude that the optical properties of silver nanoparticle arrays have been definitely changed due to the oxidation.

Comparing Fig. 4 with Fig. 6 and Fig. 7, we can see the changes of extinction spectra are basically same. The experimental results demonstrate that the measured spectrums are basically in agreement with the theoretical spectrums derived by the DDA calculation. So the hybrid Au-Ag nanoparticles with a thin film of gold deposited on top of the silver nanoparticles can prevent oxidation and the positions of peak wavelengths are basically consistent with pure silver nanoparticles.

Fig. 8 shows the SEM images of hybrid Au-Ag nanoparticle arrays for different thicknesses (the gold film thickness are fixed on 5 nm). As shown in Fig. 8(a), the hybrid Au-Ag nanoparticles exhibit a hexagonally arranged disc structure rather than triangular structure, as the thickness of deposited hybrid film is 30 nm. When the hybrid Au-Ag nanoparticles arrive at the glass substrate after passing through the triangular gaps, the energy falls sharply. In this case, the disc structure is easier formed because of its smaller surface energy. Besides, as the prior deposition particle has been combined with the substrate and no subsequent particle proceeds, the smaller disc structure can't spread out into the triangular one. However, as the deposited film thickness increases, the angular structure mounts, and tends to regular, which is presented as in Figs. 8(b) and 8(c). As shown in Fig. 8(c), the angular structure turns into regular. This structure is very conducive to further modification experiments for signal detection. Fig. 8(d) shows the SEM image of hybrid Au-Ag nanoparticle arrays with the hybrid film of 45 nm thickness. In this case, the triangular array is evident. However, the array is not as regular as those shown in Fig. 8(c). This is mainly because of the deposition time, which determines the thickness of the film. Firstly, the evaporation hybrid Au-Ag particles cover the gap interspaces among the spheres, and the energy reduces greatly. Secondly, the subsequent particles combine with the advanced ones to form larger particles. Thirdly, when more and more particles accumulate, they may collapse in the triangular

gaps. As their energy in the second process has decreased, the collapsed particles cannot combine with the substrate further more. So, the particles can't spread out into the regular triangular array, which is shown in Fig. 8(c).

To further confirm that the difference morphologies of the nanoparticle arrays originates from the thickness of the deposition films, as shown in Fig. 9, the SEM images of the films with the thickness of 40 nm and 45 nm are compared before the removing of PS nanospheres. For the case of 40 nm in Fig. 9 (a), it is clear that the hybrid Au-Ag nanoparticles only cover the gaps and the surface of the PS spheres, while the triangular gaps is not full, and the subsequent nanoparticles can still fill up the hollowness. As the thickness of the hybrid film increases to 45 nm, both the PS spheres and the gaps interspaces are covered up with hybrid Au-Ag nanoparticles unevenly. Specially, the hybrid Au-Ag nanoparticles overlap the gaps interspaces. There are no more concave gaps for the subsequent nanoparticles. Thus, the triangular structure is defective and non-uniform, just as seen in Fig. 8(d).

The actual heights of the triangular hybrid Au-Ag nanoparticles are further characterized by AFM, as shown in the Fig. 10. Fig. 10(a) shows the 2D AFM image of the nanoparticle arrays for 30 nm average thickness film. It can be seen that the triangular structure array is irregular, with rough surface and many tiny dispersed particles. Figs. 10(b) and (c) show the AFM images of the silver nanoparticle arrays for 35 nm and 40 nm average thickness film, respectively. Both results show a hexagonal arranged triangular structure as a whole. The hybrid Au-Ag nanoparticles combine with the substrate in regular triangular. In these cases, the surfaces are smooth and no obvious dispersed particles. Fig. 10(d) shows the AFM image for the 45 nm average thickness film. In comparison with the samples of 35 nm and 40 nm, although the array in Fig. 10(d) keeps regular, each hybrid Au-Ag triangular nanoparticle shows imperfect with its triangular column growing upwards. The label D_t in Fig. 10 represents the nanoparticle for height measuring. The measured heights are (a) 28 nm, (b) 34 nm, (c) 40 nm and (d) 44 nm, respectively. The difference between the single nanoparticle measured value and array measured average value is due to the fact that surface of nanoparticle array fabricated is not entirely uniform and flat.

The dielectric constants of noble metal nanoparticle is different from substrate. When the substrate is considered in DDA calculation model, the calculated results is different from non-substrate model. When measuring the extinction spectra of samples, we use a blank glass as reference and the spectras obtained have subtracted the background absorbance of the blank glass. In order to make the comparison between calculation and experimental measurement results under the same conditions, in DDA calculation. We use non-substrate model to reduce error caused by substrate effect.

Figs. 11(a)-11(d) shows experimental and the calculated extinction spectras of hybrid Au-Ag nanoparticle arrays for different thicknesses (a) 30 nm; (b)

35 nm; (c) 40 nm and (d) 45 nm. Compared to the calculated results, experimental peaks appear 38 nm, 33 nm, 26 nm and 34 nm blueshifts, respectively, as shown in Figs. 11(a)-11(d). As can be seen from Figs. 11(a)-11(d), we can find the calculated results of the plasmon wavelength with the designed model agree with the experimental measured results of spectrums.

The only major difference with the experiment is that the experimental peaks appear 26 nm to 42 nm blueshifts compared to the calculated results. The reason is likely to be that fabrication error causes uniformity issue for both size and shape of the particles. In addition, in DDA calculated model, the edge of the triangular nanoparticles is straight while in experiment it is curving. From Fig. 11(c), it can be seen apparently that when the wavelength is 661 nm, the extinction efficiency reaches to a maximum value. When DDA calculation is taken to calculate the extinction efficiency, the maximum wavelength of extinction efficiency is 687 nm. The changes of theoretical and experimental spectras are basically consistent. The only major difference with the experiment is that the experimental peaks appears 26 nm blueshift compared to the calculated result and the shift of the peak wavelength is minimum among the experimental spectras.

Most of the results presented here are analysis and characterization of the thickness variation and array period. The results for the 2D hexagonally arranged triangular hybrid Au-Ag nanoparticle arrays show that parameters of 40 nm thickness can be used in our experimental fabrication. The experimental results are generally in agreement with the calculated results.
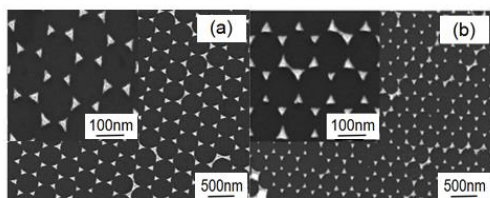
Fig. 5. The SEM images of (a) pure silver nanoparticle arrays and (b) hybrid Au-Ag nanoparticle arrays.
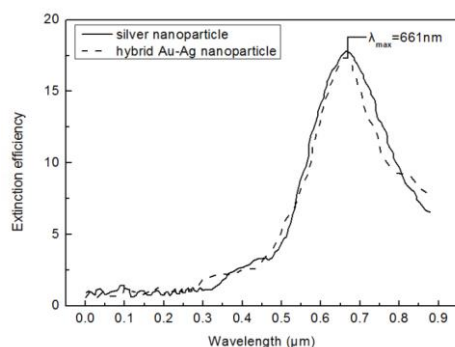
Fig. 6. UV–vis spectra of pure silver nanoparticle arrays (sample a) and hybrid Au-Ag nanoparticle arrays (sample b).
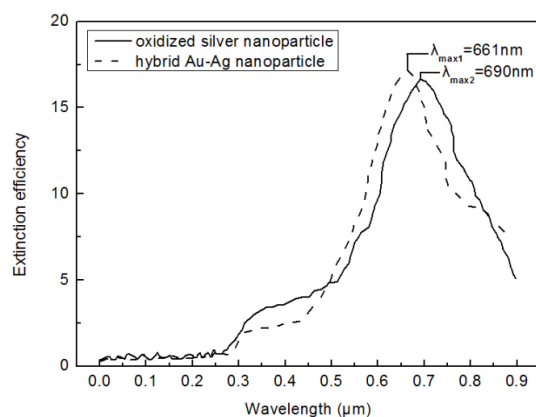
Fig. 7. UV–vis spectra of pure silver nanoparticle arrays (sample a) and hybrid Au-Ag nanoparticle arrays (sample b) exposed to air.
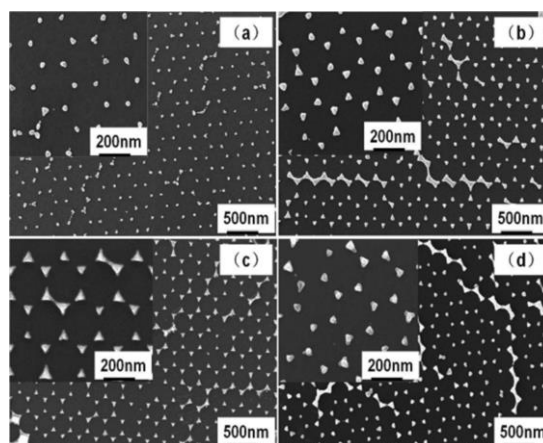
Fig. 8. The SEM images of hybrid Au-Ag nanoparticle arrays for different thicknesses (a) 30 nm; (b) 35 nm; (c) 40 nm and (d) 45 nm.
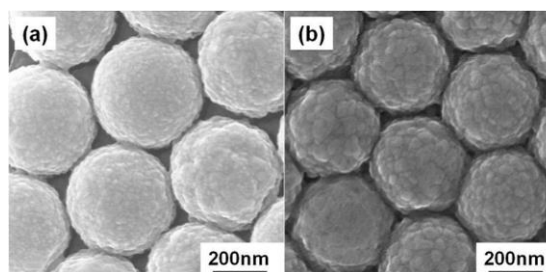
Fig. 9. Representative SEM images of the gas interspaces among the PS spheres deposited with different thicknesses of films: (a) 40 nm; (b) 45 nm.
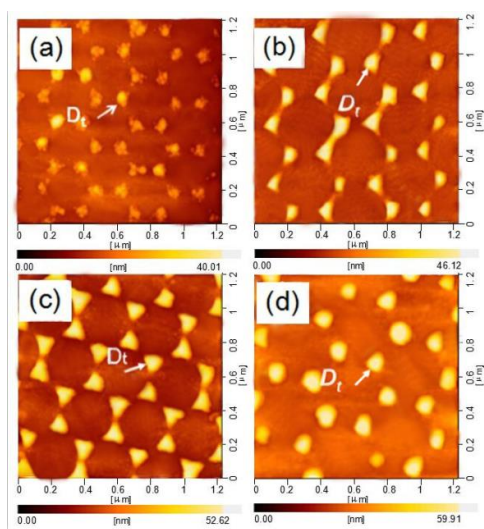
Fig. 10. AFM images of the hybrid Au-Ag nanoparticle arrays for different thicknesses: (a) 30nm; (b) 35nm; (c) 40nm; (b) 45nm.
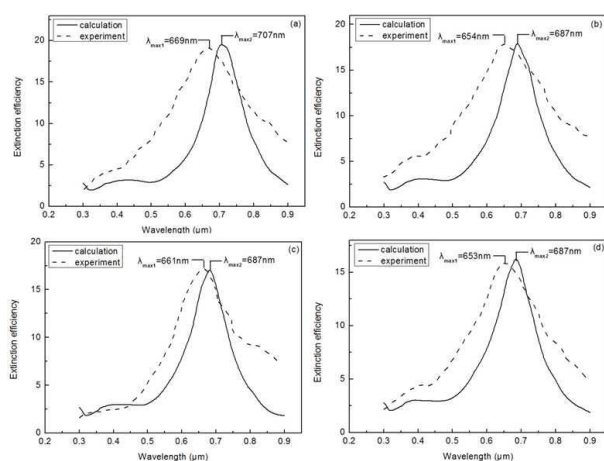
Figs. 11(a)-11(d). Experimental and the calculated extinction spectras of hybrid Au-Ag nanoparticle arrays for different thicknesses: (a) 30 nm; (b) 35 nm; (c) 40 nm and (d) 45 nm.

5. Conclusion

The hybrid Au-Ag nanoparticles with a thin film of gold deposited on top of the silver nanoparticles can prevent oxidation and keep the stability. The particle thickness has important effect on optical properties of the hybrid nanoparticle arrays. Both theoretical calculations and experimental results demonstrate 40 nm thickness can be used as parameters for the hybrid nanostructure and the parameters can be used to fabricate hybrid Au-Ag triangular nanoparticle arrays with regular angular structure. The experimental results demonstrate that the measured spectrums are basically in agreement with the theoretical spectrums derived by the DDA calculation.

References

[1] L. Wang, Appl. Phys. A **102**, 121 (2011).
[2] C. L. Haynes, R. P. Van Duyne, Nano Lett. **3**, 939 (2003).
[3] Y. J. Xiong, R. Long, D. Liu, X. L. Zhong, C. M. Wang, Z. Y. Li, Y. Xie, Nanoscale **4**, 4416 (2012).
[4] A. J. Haes, W. Paige Hall, C. Lei, W. L. Klein, R. P. Van Duyne, Nano Lett. **4**, 1029 (2004).
[5] T. Ayako, N. Kazuki, K. Norihisa, Adv. Mater. **25**, 3197 (2013).
[6] M. Shunsuke, F. Yutaka, L. Koji, T. Katsuhisa, Appl. Phys. Lett. **98**, 121917 (2011).
[7] M. K. Fan, M. Thompson, M. L. Andrade, A. G. Brolo, Anal. Chem. **82**, 6350 (2010).
[8] A. Singh, J. Jayabalan, R. Chari, H. Srivastava, S. M. Oak, J. Phys. D: Appl. Phys. **43**, 335401 (2010).
[9] S. Samanta, P. Sarkar, S. Pyne, G. P. Sahoo, A. Misra, J. Mol. Liq. **165**, 21 (2012).
[10] R. C. Jin, Y. W. Cao, C. A. Mirkin, K. L. Kelly, G. C. Schatz, J. G. Zheng, Science **294**, 1901 (2001).
[11] B. T. Draine, P. J. Flatau, J. Opt. Soc. Am. A **11**, 1491 (1994).
[12] N. Geuquet, L. Henrard, Ultramicroscopy **110**, 1075 (2010).
[13] Y. J. Song, H. E. Elsayed-Ali, Appl. Surf. Sci. **256**, 5961 (2010).
[14] C. C. Kao, Y. K. Su, C. L. Lin, J. J. Chen: IEEE Photonics Technol. Lett. **22**, 984 (2010).
[15] T. R. Jensen, M. D. Malinsky, C. L. Haynes, R. P. Van Duyne: J. Phys. Chem. B **104**, 10549 (2000).
[16] B. T. Draine, P. J. Flatau, User Guide for the Discrete Dipole Approximation Code DDSCAT.7.3.0, 2013.
[17] P. C. Chaumet, A. Rahmani, G. W. Brvant, Phys. Rev. B **67**, 165404 (2003).
[18] S. Samanta, P. Sarkar, S. Pyne, G. P. Sahoo, A. Misra, Journal of Molecular Liquids **165**, 21 (2012).
[19] P. Sarkar, D. K. Bhui, H. Bar, G. P. Sahoo, S. Samanta, S. Pyne, A. Misra, Plasmonics **6**, 43 (2011).
[20] L. P. Jiang, S. Xu, J. M. Zhu, J. Zhang, H. Chen, Inorganic Chemistry **43**, 5877 (2004).
[21] B. Tang, J. An, X. L. Zheng, S. P. Xu, D. M. Li, J. Zhou, B. Zhao, W. Q. Xu, Journal of Physical Chemistry C **112**, 18361 (2008).
[22] J. Liu, Xiamen University (2014).

_____

*Corresponding author: jingliu@jmu.edu.cn